Large-Scale Modulation of Mesoscale Convective System Propagation and Diurnal Rainfall over the Western Maritime Continent

Zhenyu You[a, b], Pu Lin[a, b], Simon Peatman[c], Hugh Zhang[c], and Yi Ming[a, b]

a. Department of Earth and Environmental Sciences, Boston College, Chestnut Hill, MA

b. Schiller Institute for Integrated Science and Society, Boston College, Chestnut Hill, MA

c. Centre for Climate Research Singapore, Meteorological Service Singapore, Singapore

Corresponding author: Zhenyu You (zhenyu.you@bc.edu)

Preprint statement:

This is a non-peer-reviewed preprint submitted to EarthArXiv. The manuscript has been submitted to *Journal of Climate* for peer review.

ABSTRACT

The western Maritime Continent exhibits a pronounced regional diurnal cycle of rainfall, to which the propagating Mesoscale Convective Systems (MCSs) make a significant contribution. Using an automated tracking algorithm based on brightness temperature, we quantify the contribution of MCSs to the regional diurnal cycle over Singapore and the South China Sea. MCSs affecting the Singapore sector show two distinct peaks in the diurnal cycle, one in the early morning and the other in the afternoon. These two diurnal peaks reflect the superposition of two opposing MCS propagation pathways: eastward-propagating events originating from Sumatra and westward-propagating events originating from the South China Sea and Borneo, respectively. These propagation regimes occur under systematically different large-scale wind profiles. Eastward and westward propagation are associated with distinct lower- and mid-tropospheric zonal wind conditions, whereas upper-tropospheric winds provide less separation between the two regimes. Seasonal changes in MCS directionality are consistent with changes in the preferred low-level wind direction. The Madden-Julian Oscillation (MJO) modulates the relative frequency of eastward- and westward-propagating events and thereby influences the regional diurnal cycle through its effect on the environmental wind profiles. These results show that the regional diurnal cycle over the western Maritime Continent is shaped not only by local land-sea thermal contrasts but also by distinct populations of propagating MCSs whose preferred pathways are modulated by the large-scale environment.

SIGNIFICANCE STATEMENT

Rainfall near Singapore and the South China Sea does not follow a single daily cycle. It is the consequence of two different storm pathways, with one group moving eastward from nearby Sumatra and another moving westward from Borneo and the South China Sea. These two storm populations peak at different times of day and together regulate the regional daily rainfall cycle. Their preferred propagation directions are linked to differences in the environmental wind profile, which is modulated by large-scale tropical variability such as the Madden-Julian Oscillation. Therefore, the daily rainfall cycle in the western Maritime Continent depends on large-scale atmospheric conditions. Capturing this connection is important for simulating regional rainfall variability in weather and climate models.

1. Introduction

In the tropics, the diurnal cycle of convective activity and precipitation is a fundamental mode of atmospheric variability and is especially pronounced in coastal and archipelagic regions with complex topography (Yang and Slingo 2001). The Maritime Continent exhibits exceptionally strong diurnal rainfall variability because its dense distribution of islands and shallow seas creates sharp land-sea thermal contrasts and vigorous coastal circulations (Neale and Slingo 2003; Sakaeda et al. 2017, 2020). Over islands and coastal regions, daytime solar heating destabilizes the boundary layer over land, while sea-breeze and mountain-valley convergence favor convective initiation. Overnight, the reversal of coastal circulations together with enhanced nighttime low-level convergence over water favors rainfall over the adjacent seas (Mori et al. 2004; Ichikawa and Yasunari 2006, 2008). Because of its large amplitude, the diurnal cycle accounts for a substantial fraction of regional rainfall variability and projects strongly onto the mean precipitation over the Maritime Continent (Neale and Slingo 2003). Yet models still struggle to represent both the phase and amplitude of this cycle (Neale and Slingo 2003; Love et al. 2011; Christopoulos and Schneider 2021; Tang et al. 2021; Watters et al. 2021), and these errors contribute to substantial biases in mean rainfall and latent heating over the Maritime Continent, which can also affect remote regions through planetary wave responses (Neale and Slingo 2003; Love et al. 2011).

The diurnal cycle is shaped not only by convection that forms and rains locally, but also by *organized propagating systems* that move away from their genesis regions. Among the most important of these are Mesoscale Convective Systems (MCSs), which typically span hundreds of kilometers and consist of convective cores embedded within broad stratiform rain areas that persist well after initiation (Mapes and Houze 1993; Houze 2004, 2018). Over the Maritime Continent, MCSs often develop over islands during late afternoon and early evening before moving offshore overnight (Mori et al. 2004; Ichikawa and Yasunari 2006; Wu et al. 2009; Yokoi et al. 2019). A prominent example is Sumatra squalls, eastward-propagating lines of thunderstorms that typically initiate over Sumatra or the Strait of Malacca, cross Peninsular Malaysia and Singapore, and continue into the South China Sea (Lo and Orton 2016; Chan et al. 2019; Nguyen et al. 2025). These squalls are often accompanied by heavy rainfall and strong near-surface wind gusts that substantially disrupt regional aviation and maritime operations (Lo and Orton 2016). They usually reach Singapore in the early morning, several hours after their initial development (Lo and Orton

2016; Nguyen et al. 2025). Thus, the diurnal rainfall cycle at a given location depends not only on local convective initiation, but also on the timing, pathway, and frequency of propagating MCSs that arrive from their genesis regions.

The propagation of MCSs has been attributed to several processes that are likely to act together rather than in isolation. In squall-like MCSs, cold-pool outflows can trigger the successive regeneration of convective cells ahead of the main rain area, while low-level wind shear helps organize the convective line and sustain propagation in a preferred direction (Moncrieff and Miller 1976; Rotunno et al. 1988; LeMone et al. 1998; Weisman and Rotunno 2004). In coastal environments, diurnal terrain heating or earlier convection can also generate gravity waves that propagate away from their source. These waves can precondition the surrounding environment for convection and trigger new cells ahead of the parent system (Mapes 1993; Mapes et al. 2003; Love et al. 2011; Peatman et al. 2023). Both mechanisms explain rainfall propagation beyond simple advection and highlight the important role of the background wind profile, which influences the organization and propagation of convection along cold-pool boundaries and the dynamical and thermodynamic response to gravity-wave forcing. Consistent with this view, previous studies have shown that offshore rainfall migration around Sumatra, Borneo, and New Guinea occurs preferentially on different coasts under different wind regimes (Ichikawa and Yasunari 2006, 2008; Yanase et al. 2017; Yokoi et al. 2019).

This sensitivity to the environmental wind profile provides a natural link between MCS propagation and large-scale atmospheric variability. If changes in the wind profile favor one propagation pathway over another, large-scale disturbances that systematically alter the profile should also affect the preferred direction of MCS propagation, and, in turn, the regional diurnal cycle. Existing studies have already shown that the Madden-Julian Oscillation (MJO) and other equatorial waves modulate the phase and amplitude of diurnal rainfall over the Maritime Continent (Peatman et al. 2014, 2015; Vincent and Lane 2016; Dias et al. 2017; Sakaeda et al. 2017, 2020). However, this modulation has been examined mostly in terms of rainfall amount, cloud type, and land-sea contrasts. Recent work has further shown that the MJO and equatorial waves can modulate MCS propagation speed over Southeast Asia (Crook et al. 2024). But it remains unclear how the preferred direction of MCS propagation changes with the large-scale dynamical environment and how these changes modify the regional diurnal cycle.

To address these issues, this study examines the propagation characteristics of MCSs over the western Maritime Continent and investigates how MCS populations with different propagation directions contribute to the regional diurnal cycle. We focus on the western Maritime Continent, with particular attention to Singapore and the adjacent South China Sea, where offshore convective systems from both Sumatra and Borneo frequently converge over this important corridor for aviation and maritime traffic. Using a tracking-based climatology, we identify the dominant propagation regimes and quantify their separate contributions to the regional diurnal cycle. We then compare the environmental wind profiles associated with these regimes to assess how different background wind conditions favor eastward or westward propagation. Finally, we examine how the MJO changes the frequency of these regimes through its modulation of the environmental wind field. Section 2 describes the data and methodology, including the tracking algorithm and the climatology of MCSs over the western Maritime Continent. Section 3 presents the results for the Singapore-South China Sea sector. Section 4 provides the discussion and conclusions.

2. Methodology

a. Data

MCSs in the present study are identified using the NCEP/CPC merged geostationary satellite infrared brightness temperature (T_b) dataset (Janowiak et al. 2001, 2017). This dataset merges observations from all available geostationary satellites and has an approximately 4-km spatial resolution and a 30-min temporal resolution. This dataset has been shown to be suitable for tracking deep convective systems (e.g., Feng et al. 2021; You and Deng 2022).

For the large-scale environmental fields, this study uses the fifth-generation ECMWF atmospheric reanalysis data (ERA5), with a horizontal resolution of 0.25°×0.25° (Hersbach et al. 2020). For precipitation, we use version 7 of the Integrated Multi-satellitE Retrievals for GPM (IMERG) Final Run, produced by NASA's Precipitation Processing Center (Huffman et al. 2023). IMERG provides satellite-based precipitation estimates at a 0.1°×0.1° spatial resolution and a 30-min temporal resolution. MJO phases are defined using the daily Wheeler-Hendon Real-time

Multivariate MJO (RMM) index (Wheeler and Hendon 2004). Days of RMM amplitude less than 1 are excluded from the MJO analysis.

b. MCS detection method

MCSs are identified from infrared brightness temperature using the object-based tracking algorithm developed in You and Deng (2022) and You et al. (2024). At each time step, contiguous cold cloud regions with T_b < 221 K are first identified as candidate cloud objects. A candidate is then classified as a cold cloud system (CCS) if its total area exceeds 30,000 km^2. Tracks are constructed by linking CCSs between successive brightness temperature images. A CCS is treated as the same system if the overlapping area between two consecutive objects exceeds 50%, evaluated either forward or backward in time. An MCS is finally defined as a CCS that persists for at least 6 hours.

Threshold choices in T_b-based tracking vary substantially across studies because they depend on both the dataset and the scientific objective (Dias et al. 2017; Houze 2018). This issue is particularly relevant to the Maritime Continent, where upper-level clouds do not always correspond closely to the location or intensity of surface precipitation (Yamada et al. 2010; Peatman et al. 2014). We therefore adopt a strict definition with a cold cloud threshold of 221 K and a minimum area threshold of 30,000 km^2. These thresholds are stricter than those used in many tropical MCS studies (e.g., Dias et al. 2017; Cheng et al. 2023; Crook et al. 2024) and are intended to favor actively precipitating systems. In our analysis, this choice effectively removes cases with weak precipitation and yields a sample that better represents the rain-producing systems of interest.

c. Climatology of MCSs over the western Maritime Continent

MCS detection is conducted in the western Maritime Continent region (6°S–6°N, 93°–120°E) from 2000 to 2024. The climatological genesis and occurrence frequencies are computed on the 4-km brightness-temperature grid by counting MCS cloud pixels at genesis and throughout the full lifetime of each MCS, respectively (the same approach is used for the other MCS climatology maps). The resulting MCS climatology (Fig. 1) is broadly consistent with previous studies. MCS genesis is concentrated over the major terrain of Sumatra and Borneo and along their western coastal regions. Total MCS occurrence extends further offshore, especially off western Sumatra and Borneo. The genesis and occurrence patterns of MCSs agree well with earlier studies on the region's rainfall (Yang and Slingo 2001; Mori et al. 2004; Ichikawa and Yasunari 2006). The broad spatial consistency between MCS occurrence (Fig. 1b) and the precipitation distribution (Fig. 1c), particularly around Sumatra and Borneo, further suggests that the tracking captures the main rain-producing systems. Values near the boundaries of the tracking domain should be interpreted cautiously because systems entering or leaving the domain may have incomplete tracks and may be less likely to satisfy the duration threshold.

MCS activity also exhibits a pronounced seasonal cycle and substantial interannual variability across the region (Fig. 2). Over the western Maritime Continent, MCS frequency shows a modest peak during March-May and a much stronger peak from October through January. During these periods, low-level westerly and northwesterly flows in the intermonsoon seasons support convective organization and offshore propagation (Lo and Orton 2016; Lu et al. 2021; Nguyen et al. 2025). On the interannual timescale, MCS frequency closely matches the amount of precipitation (Fig. 2b). Severe drought years in this region, such as 2015 and 2019 (Anyamba et al. 2019; Ha et al. 2023), are characterized by low MCS frequency. The strong correlation between rainfall and MCS frequency in this region on monthly and interannual timescales (Figs. 2b-c) indicates that variability in organized convection is a major component of regional rainfall variability.

Within this broader domain, Singapore and the equatorial South China Sea form a particularly suitable region for examining MCS propagation. This sector lies between Sumatra and Borneo, two major MCS genesis regions in the western Maritime Continent, and is therefore affected frequently by systems propagating in multiple directions. It also forms an important corridor for regional aviation and maritime traffic, making the timing and propagation of MCSs practically important. The Results section therefore focuses on the propagation and characteristics of MCSs affecting this region.

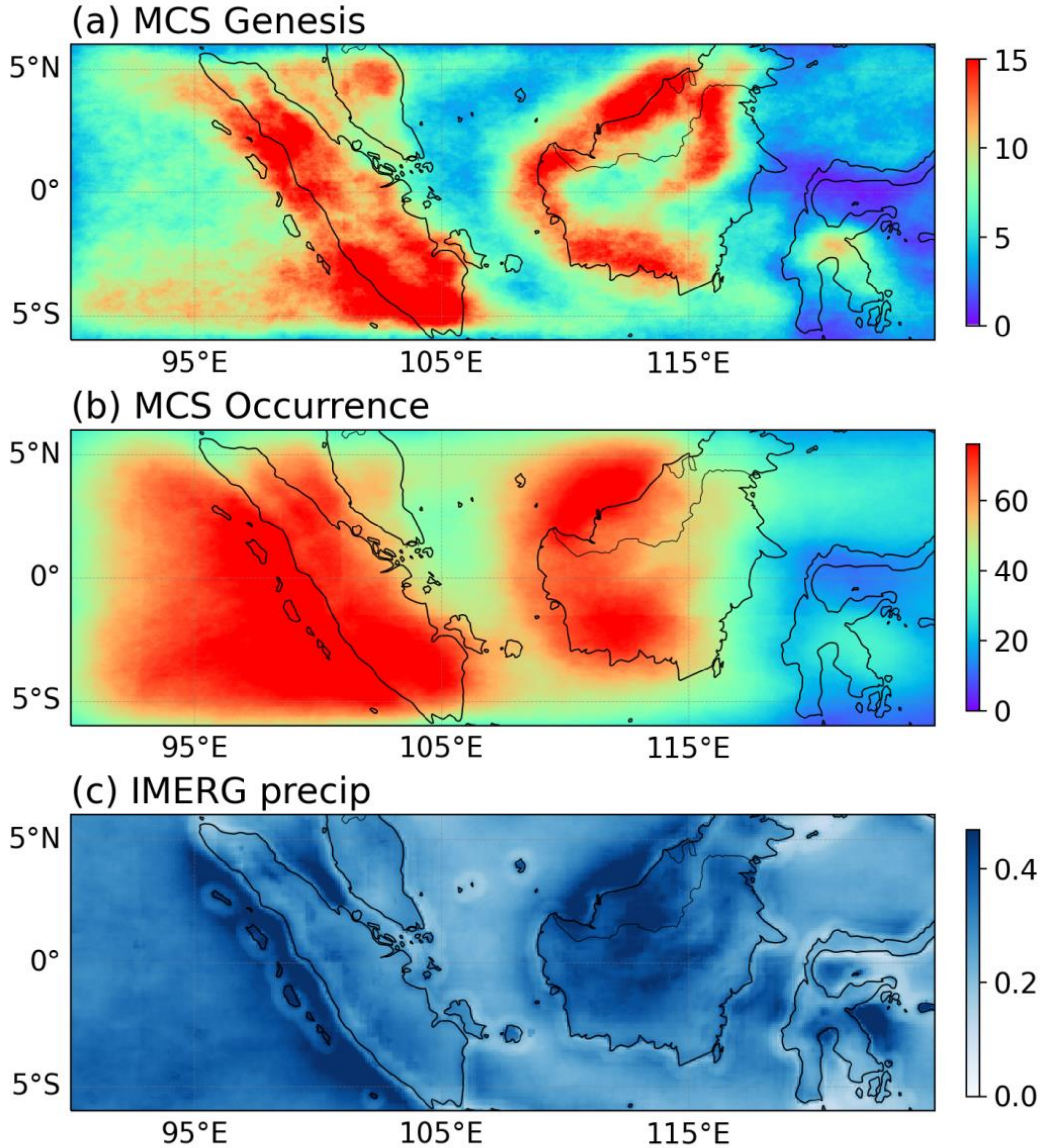

Fig. 1. Climatological distribution of MCS genesis and occurrence over the western Maritime Continent during 2000 - 2024. (a) Annual mean MCS genesis frequency and (b) annual mean MCS occurrence frequency, both expressed as counts of identified MCS cloud pixels per 0.04° × 0.04° grid cell per year. Genesis is computed from MCS cloud pixels at the first tracked time, whereas occurrence is computed from MCS cloud pixels throughout the full lifetime of each MCS. (c) Annual mean precipitation from IMERG (mm day^{-1}).

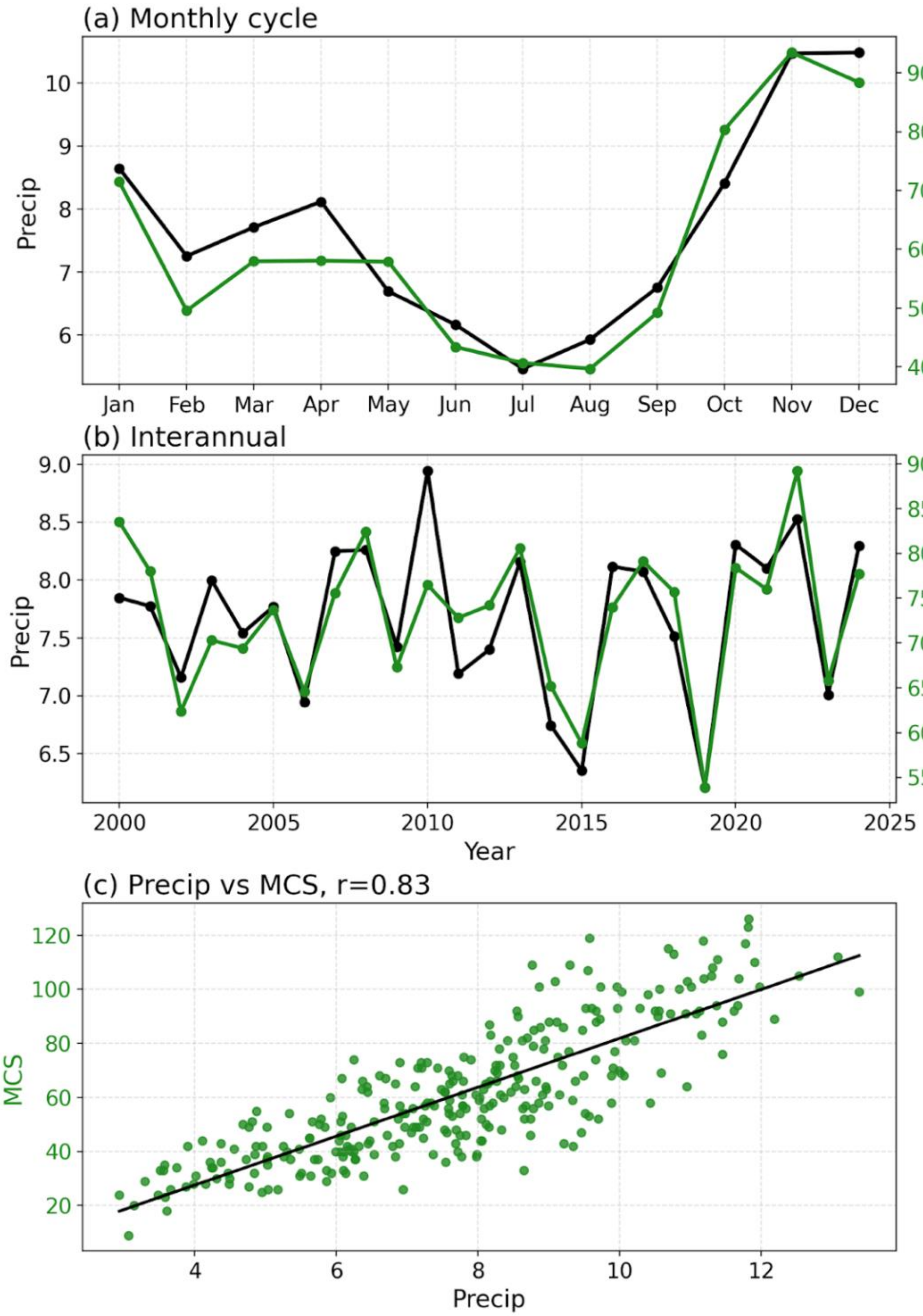

Fig. 2. Precipitation and MCS occurrence frequency over the western Maritime Continent. (a) Monthly climatology and (b) interannual time series of precipitation (mm day^{-1}; black) and MCS occurrence frequency (green). (c) Scatterplot of monthly precipitation against MCS occurrence frequency; the black line is the linear regression fit.

3. Results

a. MCS propagation and the regional diurnal cycle

We first analyze tracked MCSs whose cloud pixels overlap a box covering the Singapore sector (0°–2.5°N, 102.5°–105°E). The occurrence map for this subset shows a footprint extending from central Sumatra across the Malay Peninsula into the equatorial South China Sea (Fig. 3a). The annual cycle of this subset (Fig. 3b) follows the seasonality of MCS activity over the western Maritime Continent discussed in Section 2 (Fig. 2a).

The diurnal cycle of MCS occurrence within the Singapore box has an interesting double-peak pattern (Fig. 3c). The early-morning maximum is consistent with the timing of eastward-propagating convection from Sumatra (Mori et al. 2004; Lo and Orton 2016; Nguyen et al. 2025). If this Sumatra-origin population were the only contributor, however, the local MCS cycle would be expected to show only a single morning peak. The additional afternoon maximum therefore points to a second population with a different timing and likely a different propagation pathway. Previous observational studies in this region have shown that diurnal rainfall migration over the Maritime Continent can occur in multiple directions, including both offshore and onshore migration around major islands (Yanase et al. 2017; Yokoi et al. 2019). The two peaks in Figure 3c thus likely reflect separate MCS populations with different propagation directions.

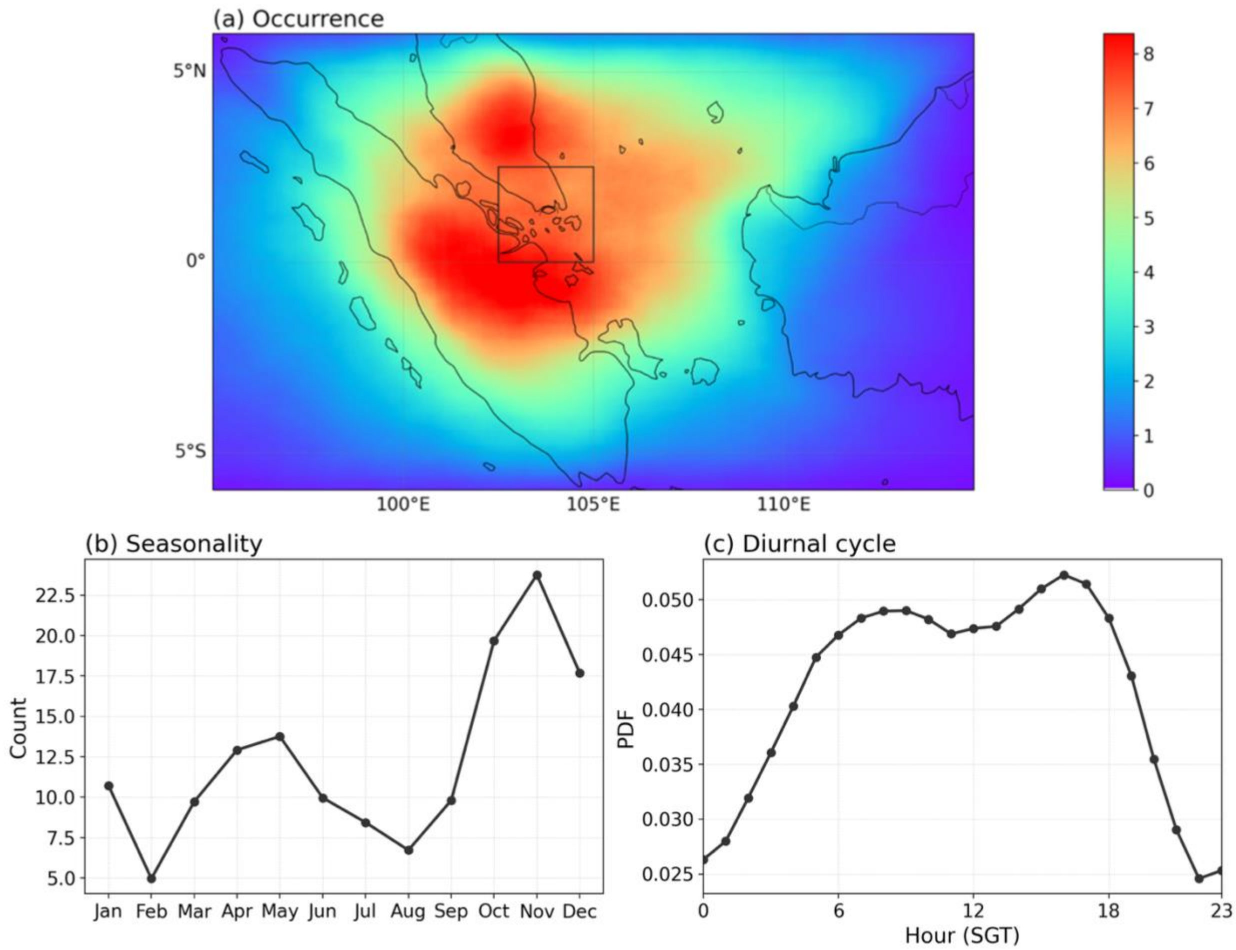

Fig. 3. MCS activity in the Singapore sector. (a) Climatological distribution of MCS cloud pixels from events overlapping the Singapore box (black box; 0°-2.5°N, 102.5°-105°E). (b) Seasonal cycle and (c) probability density function of the diurnal cycle of MCS occurrence frequency within the Singapore box.

To test this hypothesis, we divide the Singapore-sector events into the eastward- and westward-crossing categories using 104°E (approximately the longitude of Singapore) as a reference longitude (Fig. 4). Eastward events are defined as systems whose centroid longitude (averaged across all cloud pixels) is located west of 104°E at genesis and moves to the eastern side of that line by the end of the event, while westward events are defined in the opposite sense. This definition provides a relatively clean separation of systems approaching Singapore from the east and west, respectively. Note that the full cloud shield at genesis in Figure 4 can slightly extend across 104°E even when the MCS cloud centroids are all located on one side of the longitude.

The two categories show a clear contrast in genesis region, seasonality, and diurnal cycle. The genesis cloud pixels of eastward events are located mainly over Sumatra, whereas those of westward events are located primarily over the sea and coastal region to the east of the box (Fig. 4b). The seasonal activity of MCSs of both directions shows double peaks around March-June and September-November (Fig. 4c), broadly corresponding to the two monsoon-transition periods. The two curves add up closely to the total activity in Figure 3b. However, westward events show much higher activity in September-November than during the March-June peak, whereas eastward events show similar activity in the two seasons. We will demonstrate in Section 3b that this seasonal change in MCS directionality is related to changes in the preferred wind direction over this region.

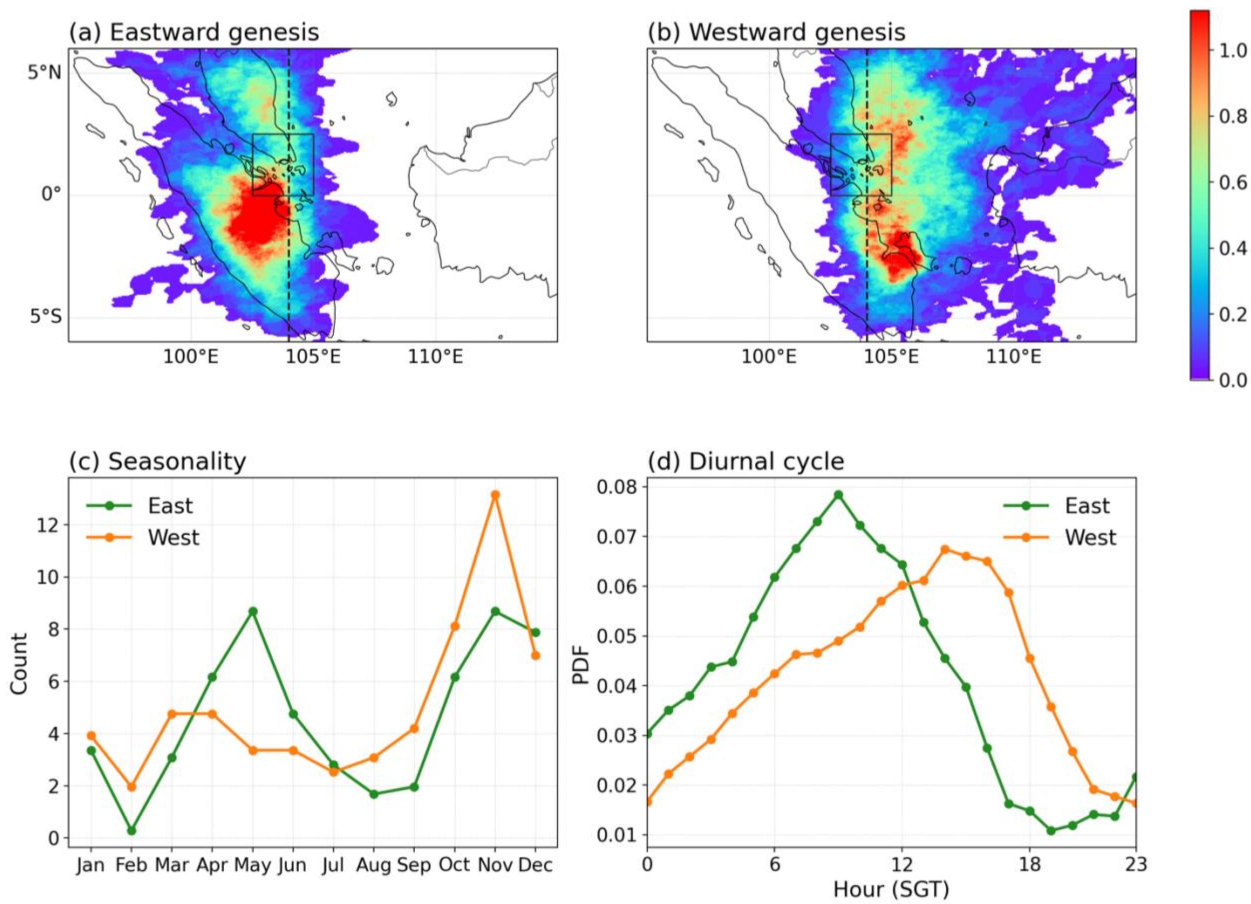

Fig. 4. Eastward- and westward-crossing MCSs affecting the Singapore sector. Climatological distribution of genesis cloud pixels for (a) eastward- and (b) westward-crossing MCSs. The vertical dashed line marks 104°E. (c) Seasonal cycle and (d) probability density function of the diurnal cycle of MCS occurrence frequency for eastward- and westward-crossing events, computed from time steps during which MCS cloud pixels overlap the black box. The black boxes in panels (a) and (b) denote the Singapore sector (0°-2.5°N, 102.5°-105°E).

Their diurnal cycles are also very different (Fig. 4d). Eastward events peak over Singapore in the early morning, while westward events peak in the afternoon. This timing difference is physically consistent with their distinct source regions and travel paths. Convective initiation over Sumatra is typically favored from late afternoon through evening due to the sea breeze and mountain-induced convergence. The convection then propagates eastward for several hours before affecting Singapore during the morning. By contrast, westward events originate from the nearby coastal and maritime region to the east and contribute primarily to the local afternoon peak. Each of these two populations corresponds to one of the diurnal cycle peaks seen in Figure 3c, showing that the local diurnal cycle over Singapore is shaped by MCS regimes with distinct propagation directions.

To place the Singapore-sector results in a broader regional context, we expand the target area eastward to the equatorial South China Sea (2.5°S-2.5°N, 103°-109°E). This larger box provides a more robust sample and is also the natural region in which to compare propagation pathways because it lies between Sumatra and Borneo. The genesis distribution already shows two preferred source regions (Fig. 5a), one over Sumatra and the other near the western coast of Borneo. The genesis regions are clearly separated when the events are grouped by eastward and westward propagation direction. For this expanded analysis, we separate events simply by their zonal displacement, with eastward events defined by an end longitude greater than the start longitude and westward events defined by the opposite. For this larger domain, this provides a clean separation of eastward- and westward-propagating systems, as shown in Figure 5c-f. In both categories, the dominant pattern is offshore propagation from the major islands into the South China Sea.

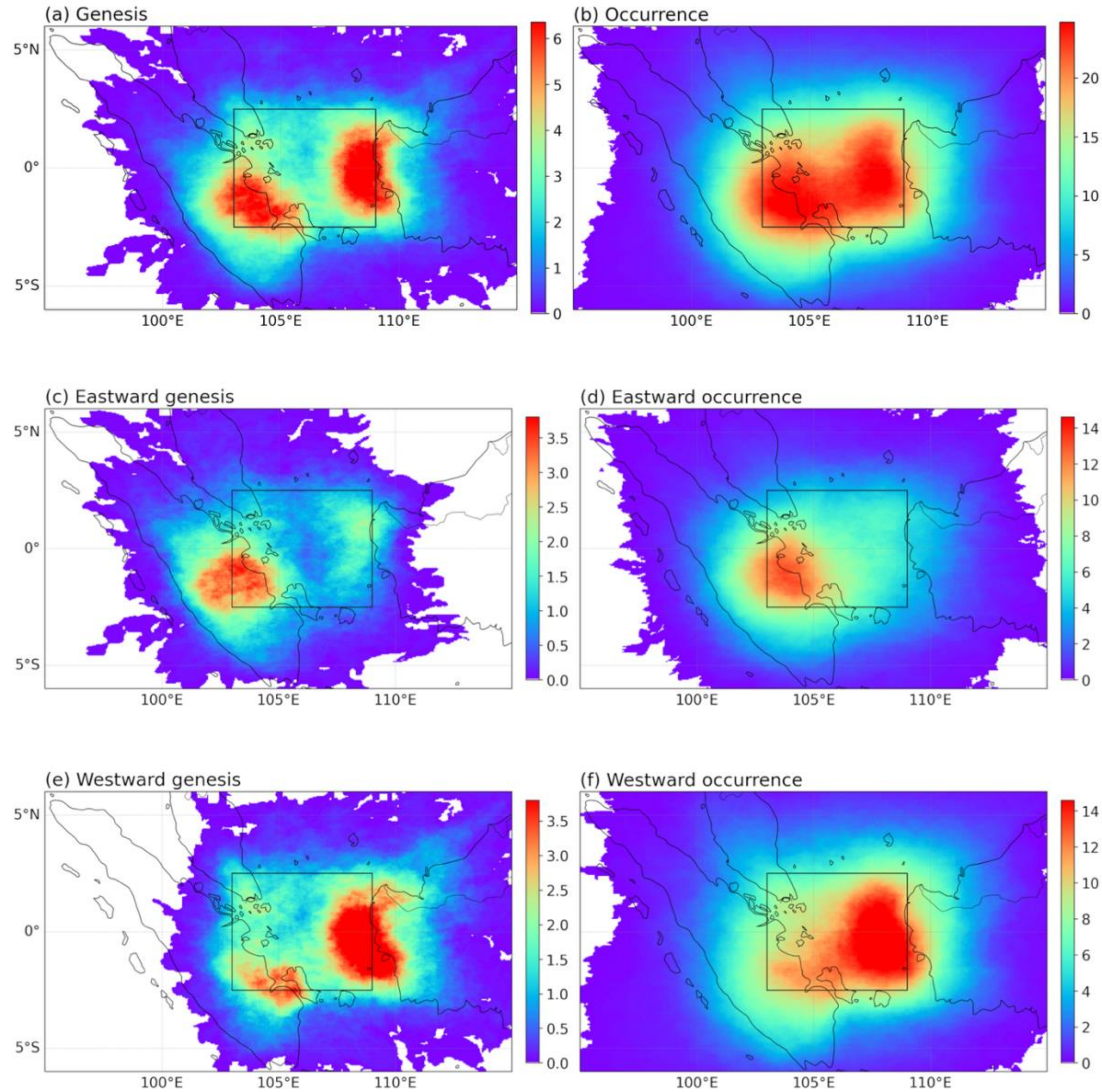

Fig. 5. Genesis and occurrence distributions of MCSs affecting the equatorial South China Sea. Climatological distribution of cloud pixels (a) at genesis and (b) during occurrence for MCSs with cloud pixels overlapping the equatorial South China Sea (black box; 2.5°S-2.5°N, 103°-109°E). (c), (d) As in (a), (b), but for eastward-propagating events. (e), (f) As in (a), (b), but for westward-propagating events.

These two categories leave markedly different footprints on the regional diurnal cycle (Fig. 6). Eastward-propagating events peak first off Sumatra and near Singapore in the early morning, and the occurrence maximum then extends further eastward into the South China Sea by late afternoon. Westward-propagating events show the reverse sequence with occurrence first peaking off the western coast of Borneo in the early morning and then extending westward toward Singapore and

Sumatra. These two populations exhibit nearly opposite diurnal evolutions, and together they produce the broader regional counterpart of the double-peak cycle identified over the Singapore box (Fig. 4c). The regional diurnal cycle is thus not simply a daily oscillation of local convective activity, but a manifestation of preferred propagation pathways that recur at characteristic times of day.

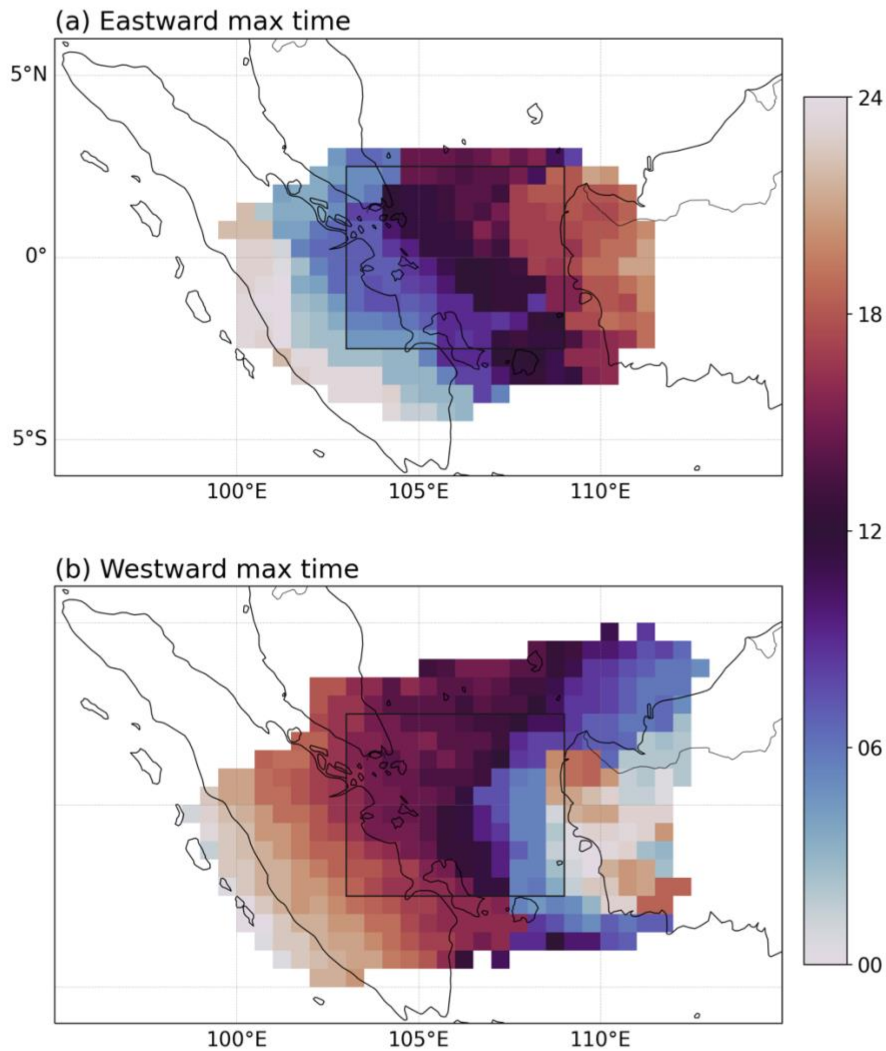

Fig. 6. Local time of maximum occurrence for MCSs overlapping the equatorial South China Sea (black box, same as in Fig. 5). (a) is for eastward- and (b) is for westward-propagating events. Times are shown in Singapore Standard Time (SGT).

Previous studies suggest that these pathways do not occur with equal frequency under all environmental conditions. Off western Sumatra, for example, nighttime offshore migration was observed on fewer than half of the observation days during the 2017 Years of the Maritime Continent (YMC) campaign and was clearly favored under specific lower-tropospheric shear conditions (Yokoi et al. 2019). On longer timescales, the likelihood of offshore propagation from Sumatra also varies with large-scale conditions under the influence of the MJO, ENSO, and the Indian Ocean Dipole (Peatman et al. 2014, 2025; Nguyen et al. 2025). Therefore, the relative importance of each regime and the corresponding timing pattern in Figure 6 can vary across a range of timescales. This highlights the importance of modulation by the larger-scale conditions, especially the environmental wind profiles, which motivates the analysis in Section 3b.

b. Environmental control of the MCS propagation direction

We first look at two representative cases, one eastward-propagating and one westward-propagating, together with their zonal wind profiles derived from ERA5 (Fig. 7). In the eastward case, the cloud and precipitation move eastward within a pronounced lower- to mid-tropospheric westerly jet extending from Sumatra into the South China Sea (Figs. 7a-b). The wind structure is consistent with the profiles generally considered favorable for Sumatra squalls (Peatman et al. 2025). In the westward case, the wind profile features mild mid-tropospheric easterlies and weak westerlies confined near the surface. In both cases, the lower-tropospheric shear is consistent with the direction of MCS propagation (Rotunno et al. 1988; LeMone et al. 1998).

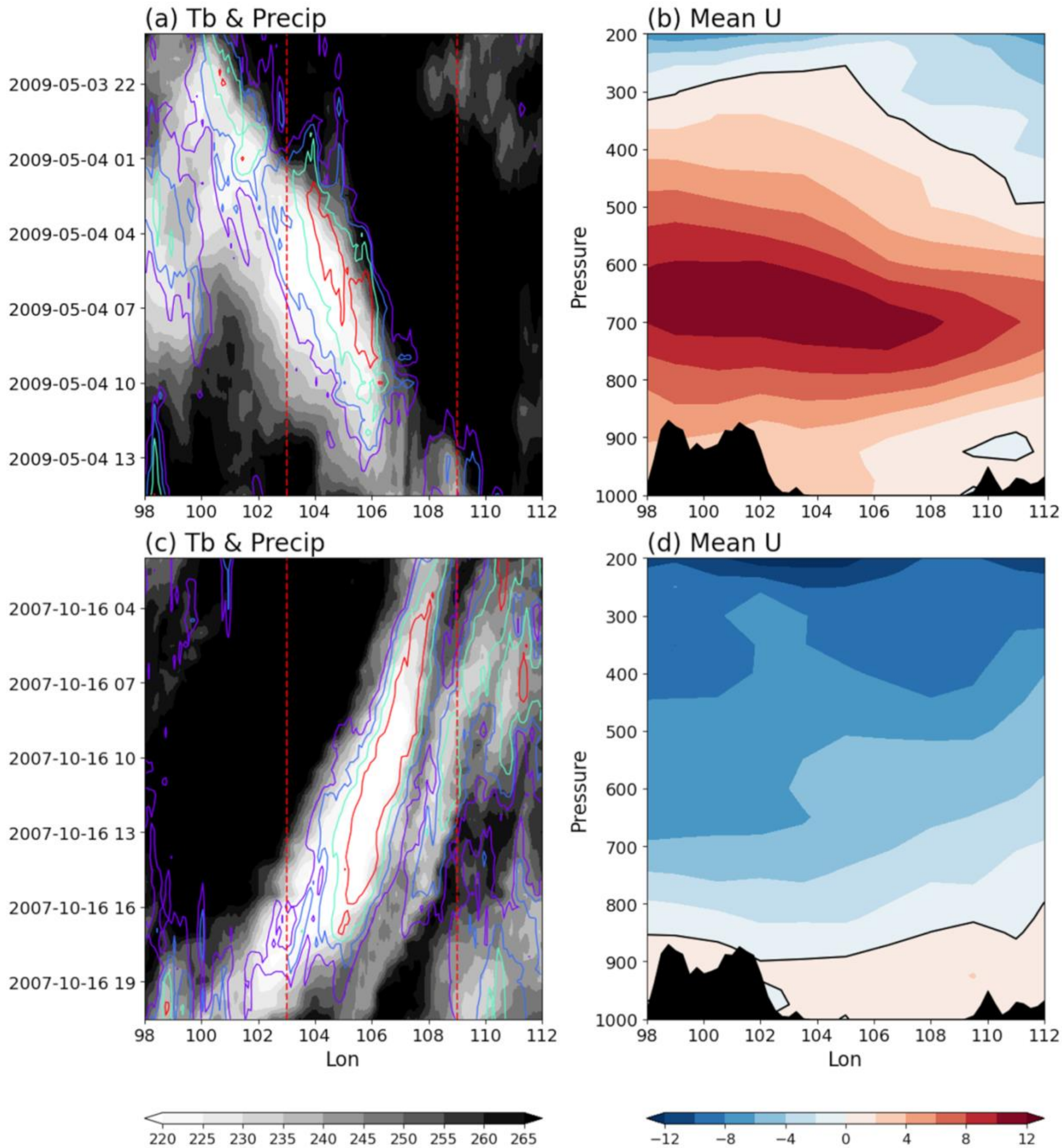

Fig. 7. Examples of eastward- and westward-propagating MCS events. (a), (c) Hovmöller diagrams of IMERG precipitation (contours; mm h^{-1}; contour interval is 2 mm h^{-1}) and brightness temperature (shading), averaged over 2°S-2°N, for the eastward- and westward-propagating cases, respectively. The two red dashed lines correspond to the western and eastern boundaries of the box in Fig. 5 (103°E and 109°E). (b), (d) Vertical cross-sections of mean zonal wind from ERA5 during the corresponding event periods, averaged over 2°S-2°N. The black areas denote terrain estimated from surface pressure averaged over 2°S-2°N.

The wind profiles of these two cases are broadly consistent with the seasonal composites (Fig. 8). Across seasons, eastward events are associated with westerly anomalies throughout the troposphere, whereas westward events show a pronounced low-level shear structure, with near-surface westerly anomalies below easterly anomalies in the mid-troposphere. The overall anomaly patterns are similar across seasons. In both propagation classes, upper-tropospheric anomalies tend to be westerly, indicating a weakening of the climatological easterlies aloft. The upper-tropospheric wind anomaly is thus not the main discriminator of MCS propagation direction in the investigated domain. As shown in Figure 9, the distributions of 700 hPa zonal wind anomalies for eastward and westward events are clearly distinct, whereas the distributions of 200 hPa zonal wind anomalies show little separation. Previous work has similarly emphasized the importance of lower-tropospheric wind structure for rainfall propagation direction, while upper-level flows can matter more for the advection of anvil clouds and stratiform structures than for the propagation of the rain-producing system itself (Yamada et al. 2010).

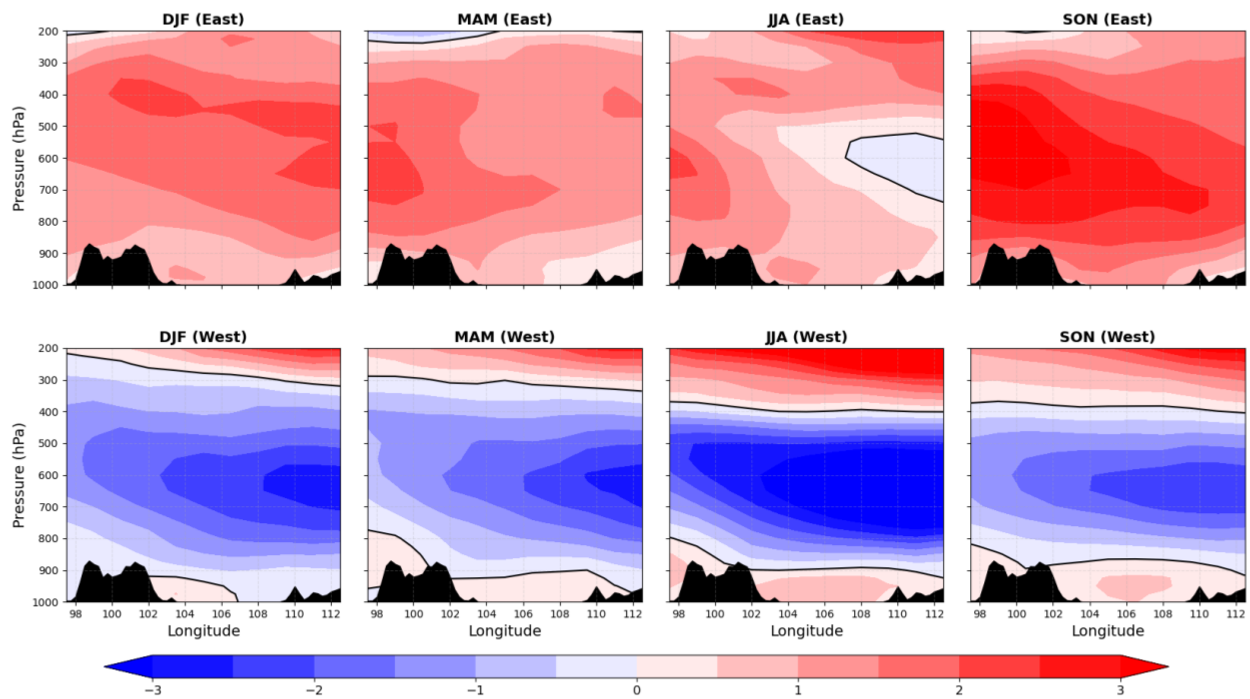

Fig. 8. Seasonal composites of zonal wind anomalies associated with eastward- and westward-propagating MCS events. Shown are vertical cross-sections of mean zonal wind anomalies (with the seasonal mean subtracted) averaged over 2°S-2°N for eastward events (top row) and westward events (bottom row). The black areas denote terrain estimated from surface pressure averaged over 2°S-2°N.

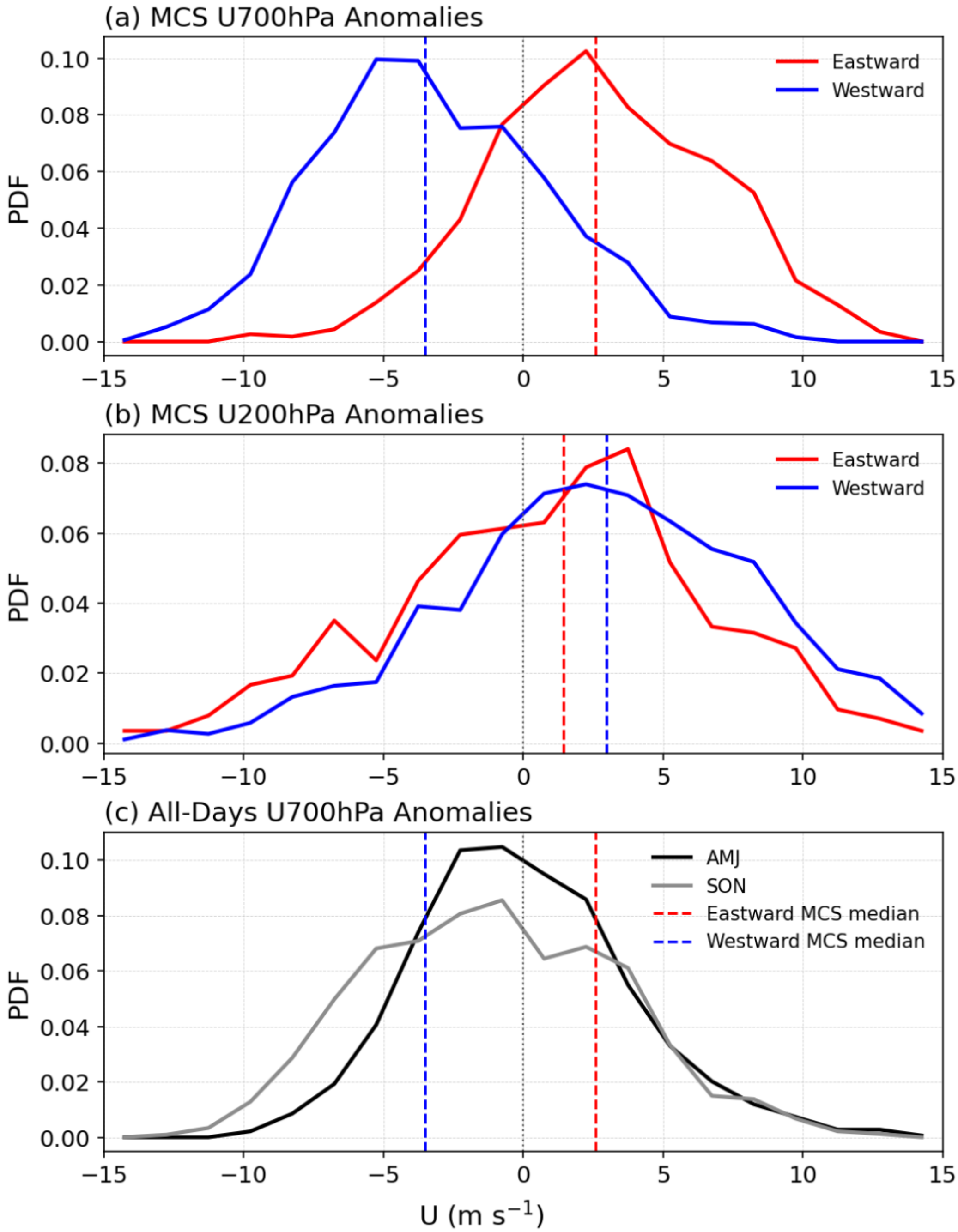

Fig. 9. Probability density functions of zonal wind anomalies associated with eastward- and westward-propagating MCS events. Zonal wind anomalies (with the annual mean subtracted) at (a) 700 and (b) 200 hPa, averaged within the black box in Fig. 5, for eastward (red) and westward (blue) events. Vertical dashed lines indicate the median values for eastward and westward events. (c) Daily 700 hPa zonal wind anomalies (with the annual mean subtracted) for April-June (AMJ; black line) and September- November (SON; gray line), averaged within the black box in Fig. 5. The vertical dashed lines are the same median values for eastward and westward events as in (a).

Seasonal changes in MCS directionality in the Singapore-South China Sea sector (not shown; qualitatively similar to Figure 4c) are consistent with changes in low-level wind direction. Figure 9c shows the daily 700 hPa zonal wind departures from the annual mean during the two periods of peak MCS activity: April-June (AMJ) and September-November (SON). The number of days with eastward wind anomalies exceeding the median value associated with eastward MCSs (red dashed line), above which eastward MCSs are much more frequent than westward MCSs (Fig. 9a), is similar in AMJ and SON. In contrast, days with westward wind anomalies stronger than the median value associated with westward MCSs are much more frequent in SON than in AMJ. This difference explains why eastward events occur at similar frequencies in AMJ and SON, whereas westward events are much more frequent in SON, as shown in Figure 4c.

It is also notable that the propagation speed of both cases in Figure 7 is about 15 m s^{-1}, clearly faster than the environmental wind in each case throughout the troposphere. These systems therefore cannot be interpreted as passive advection by the background flow alone but have their own intrinsic propagation dynamics. The speed is also of the same order as the phase speeds reported for diurnally forced gravity waves in tropical coastal regions and earlier Maritime Continent studies (Mapes et al. 2003; Love et al. 2011), suggesting that gravity waves may contribute to the rapid propagation of these events. Recent studies of offshore propagation over Sumatra indicate that coherent propagation can occur with land-breeze and cold-pool density currents maintaining the main convective line while gravity waves precondition the environment further ahead (Peatman et al. 2023, 2025). While the relative importance of these mechanisms may vary from case to case, the overall picture is that MCSs propagate through a combination of density current and gravity wave dynamics, with the environmental wind profile setting a favored direction.

c. MJO modulation of MCS propagation

Since the preferred direction of MCS propagation is closely tied to the environmental wind profile, large-scale disturbances that systematically alter that profile should also shift the relative frequencies of eastward- and westward-propagating events. We therefore examine how MCS propagation direction is affected by different phases of the MJO, the major contributor to tropical intraseasonal variability. As shown in Figure 10, the frequencies of the two propagation types vary substantially across the MJO lifecycle, defined here using the RMM index as mentioned in Section 2 (days with RMM amplitude smaller than 1 are excluded from the analysis). Previous studies of the regional diurnal cycle have generally emphasized stronger land convection ahead of the active MJO envelope and a delayed, more oceanic rainfall signal when the active envelope is over the region (Peatman et al. 2014, 2015; Sakaeda et al. 2017, 2020). In the more local Singapore-South China Sea sector considered here, the picture is not entirely consistent. Westward-propagating events (with a delayed diurnal cycle near Singapore) are most frequent in phase 2, when the main MJO convective envelope is still over the Indian Ocean and approaching the western Maritime Continent. Eastward-propagating events (with an earlier diurnal cycle near Singapore) are most frequent in phase 6, when the envelope has shifted east of the Maritime Continent into the western Pacific.

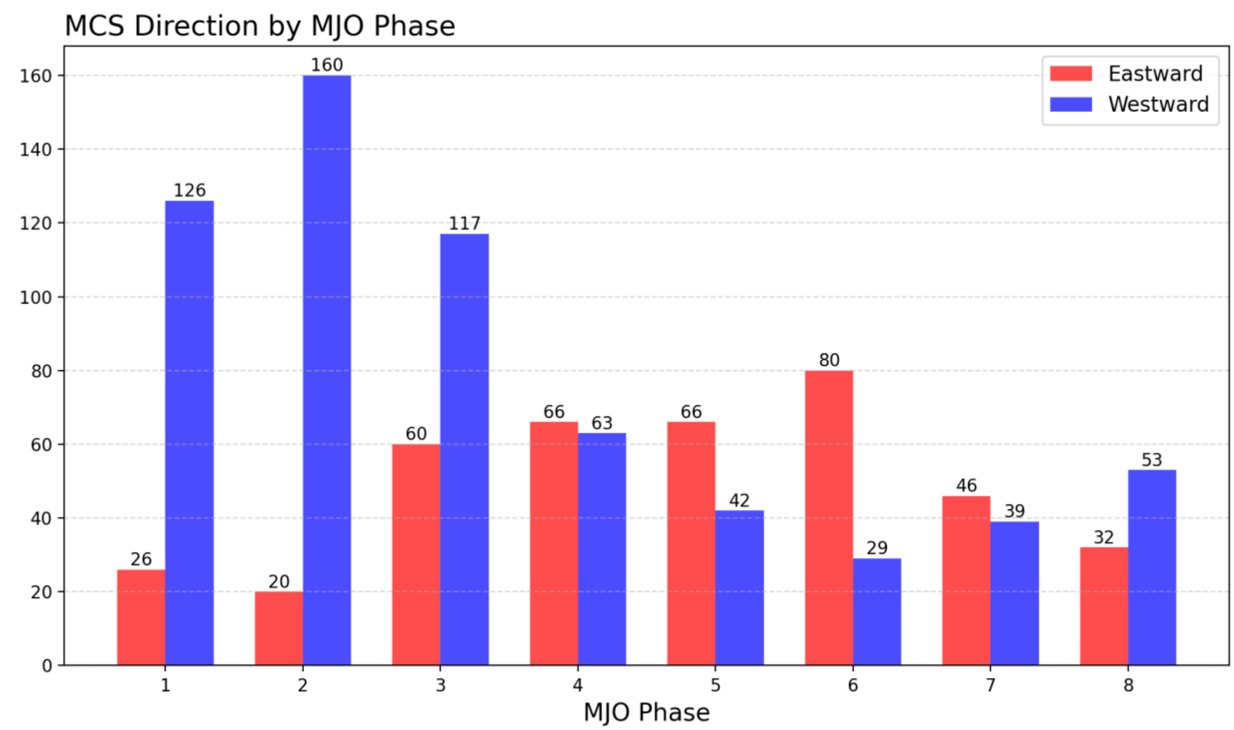

Fig. 10. Occurrence frequencies of eastward- and westward-propagating MCSs across different MJO phases, defined using the RMM index. Days with RMM amplitude smaller than 1 are excluded.

The changes in the MCS propagation direction across MJO phases are consistent with the associated atmospheric circulation anomalies. Figure 11 shows the large-scale convection and atmospheric circulation anomalies (30-90-day bandpass filtered) associated with eastward and westward events. In both lag-regression maps, the OLR anomalies show a coherent eastward-propagating convective signal characteristic of the MJO. As indicated by the low-level streamfunction, eastward events occur when the large-scale circulation favors anomalous westerly flow over the western Maritime Continent, whereas westward events occur when the circulation favors anomalous easterly flow. Therefore, on the intraseasonal timescale, the wind profile changes associated with eastward and westward cases shown in Figures 7-9 are embedded within broad circulation anomalies rather than arising purely from local changes. The preferred MCS direction over the western Maritime Continent is thus linked to large-scale disturbances such as the MJO that modulate regional atmospheric circulation. When the MJO convective envelope shifts east of the western Maritime Continent (phase 6), the low-level westerly flow is more favorable for eastward propagation into the Singapore-South China Sea sector. By the same reasoning, westward events are more prominent when the MJO convective envelope is approaching from the Indian Ocean (phase 2), when the large-scale circulation produces anomalous low-level easterlies in this sector.

Taken together, our results suggest that the MJO's influence on the regional diurnal cycle in the Singapore-South China Sea sector manifests in part through shifts in the relative importance of opposing propagation regimes under different wind conditions. While earlier studies have mainly emphasized MJO modulation of the diurnal cycle through changes in land-sea contrast and in cloud cover and cloud type (e.g., Sakaeda et al. 2017), our results add that, on a more regional scale, part of this modulation also operates through changes in the preferred propagation direction of MCSs under different environmental wind profiles. Accounting for MCS propagation is therefore important for understanding the local diurnal cycle. This finding also points to a potential source of predictability, because changes in the regional diurnal cycle could be anticipated from the evolving state of the large-scale atmospheric circulation.

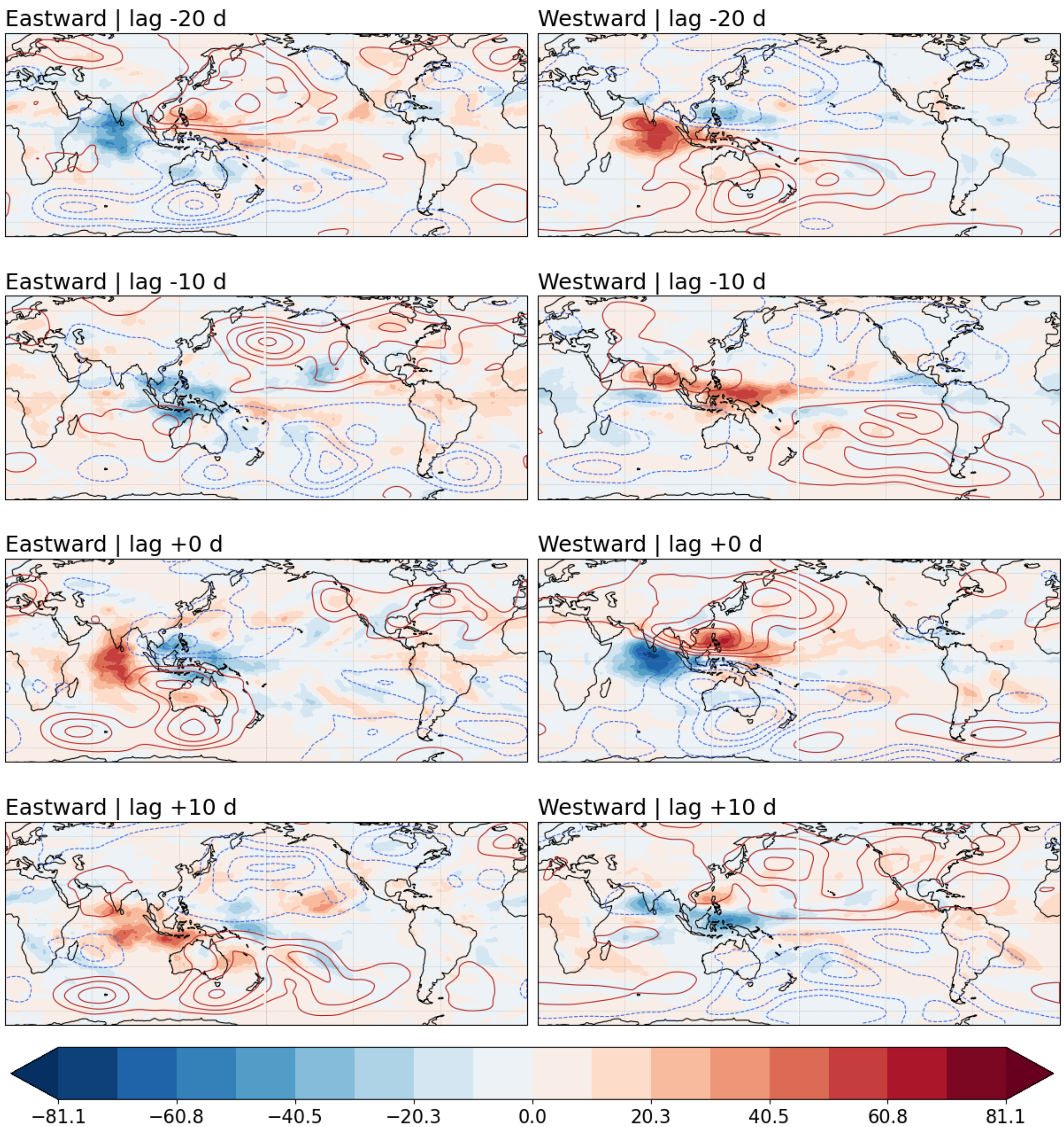

Fig. 11. Intraseasonal circulation and convection anomalies associated with eastward- and westward-propagating MCS activity. Lag regressions of 30–90-day bandpass-filtered OLR (shading; W m^{-2}) and 700-hPa streamfunction (contours; m^2 s^{-1}; blue dashed for negative anomalies and red solid for positive anomalies; contour interval is 2.8×10^6 m^2 s^{-1}) onto the occurrence frequency of eastward-propagating MCSs (left column) and westward-propagating MCSs (right column).

4. Concluding Remarks

Using a brightness-temperature-based tracking climatology, this study examined how propagating MCSs shape the diurnal cycle over the western Maritime Continent. We focused on the events affecting Singapore and the South China Sea sector, where organized convection from both Sumatra and Borneo frequently propagates. The results show that the regional diurnal cycle over the western Maritime Continent cannot be understood as a purely local response to land-sea thermal contrast. In the Singapore sector, MCS occurrence exhibits two preferred peaks in local time, produced by two MCS populations with opposite propagation directions. Eastward-propagating systems originate primarily over Sumatra and contribute most strongly to the early morning peak, while westward-propagating systems form over the South China Sea and Borneo and contribute most strongly to the afternoon peak. A similar conclusion holds when the analysis is expanded to the equatorial South China Sea. The regional diurnal cycle is therefore the result of a combination of MCS regimes with distinct propagation directions.

The shift between MCS propagation regimes is closely linked to the environmental wind profile. Eastward and westward propagation occur under different lower- and mid-tropospheric zonal wind conditions, while upper-level winds provide less separation between the two regimes. MCSs often propagate faster than the environmental wind throughout the troposphere, indicating that these systems have their own propagation dynamics. In this sense, the environmental wind acts less as a steering flow than as a large-scale constraint that favors one propagation pathway over another. Seasonal changes in MCS directionality are consistent with changes in the preferred wind direction, explaining why westward MCSs occur much more frequently in September-November, when anomalous low-level westward winds are more common during the Northern Hemisphere cool season. Large-scale disturbances such as the MJO can thus modulate the relative frequency of MCSs with different propagation directions by setting up different wind profiles. Westward-propagating events are favored most strongly when the MJO convection is over the Indian Ocean and reaching the Maritime Continent and the western Maritime Continent is dominated by low-level easterly anomalies, while eastward events are favored most strongly when the MJO convection has passed over the Maritime Continent into the western Pacific and low-level westerly anomalies are dominant.

Our findings suggest a useful two-step view of the tropical diurnal cycle. One part of this problem is about convective initiation, which depends more on local dynamical and thermodynamic forcing such as surface heating and coastal and topographic convergence. The second part is about the subsequent propagation of organized convection, including its preferred direction and speed, which depends more on mesoscale dynamics and the environmental wind profile and is continuously modulated by passing large-scale disturbances. Although MCSs are not merely a response to an imposed large-scale state, the slowly varying circulation anomalies considered here, such as those associated with the MJO, are often assumed to have their own dynamics beyond the feedback from convective processes. It thus remains useful to interpret the large-scale atmospheric circulation as a quasi-external constraint that systematically favors certain propagation pathways on certain timescales. This perspective also has clear implications for modeling. The realistic simulation of large-scale variability is indispensable for capturing MCS propagation and the diurnal cycle, beyond allowing the model to trigger convection at the correct local time.

The propagation mechanism of MCSs remains an important open question. Over the Maritime Continent, MCS propagation is likely maintained by a combination of cold-pool density currents and gravity-wave dynamics (Love et al. 2011; Peatman et al. 2023). It is worth noting that these two are not necessarily independent mechanisms. Some studies of squall-line MCSs have suggested that the cold pool and the associated rear-inflow could arise as part of a broad gravity-wave adjustment to convective and stratiform heating rather than being solely driven by evaporative cooling and melting beneath the stratiform region (e.g., Pandya and Durran 1996; Houze 2004). An interesting future direction will therefore be to examine how these mechanisms interact under different propagation regimes with varying environmental wind profiles and large-scale states.

Acknowledgement

The authors thank colleagues at the Centre for Climate Research Singapore (CCRS), Meteorological Service Singapore, for helpful discussions and suggestions that significantly improved the manuscript. The authors also acknowledge Boston College Research Computing for providing computational resources and support for this work.

Data Availability Statement

All data used in this study are publicly available. The atmospheric variables at pressure levels were obtained from the fifth-generation ECMWF reanalysis dataset (ERA5), available through the Copernicus Climate Data Store (https://cds.climate.copernicus.eu/datasets/reanalysis-era5-pressure-levels). Brightness temperature data were obtained from the NOAA/NCEP/CPC merged infrared brightness temperature product, archived by NASA GES DISC as the GPM_MERGIR dataset (https://disc.gsfc.nasa.gov/datasets/GPM_MERGIR_1/summary). Outgoing longwave radiation was obtained from the CERES SYN1deg product (https://ceres.larc.nasa.gov/data/). Precipitation was obtained from IMERG (https://gpm.nasa.gov/data/imerg). The Wheeler-Hendon Real-time Multivariate MJO (RMM) index used to define MJO phases was obtained from the Australian Bureau of Meteorology (https://www.bom.gov.au/climate/mjo/).

REFERENCES

Anyamba, A., and Coauthors, 2019: Global Disease Outbreaks Associated with the 2015–2016 El Niño Event. *Sci. Rep.*, **9**, 1930, https://doi.org/10.1038/s41598-018-38034-z.

Chan, M. Y., J. C. Lo, and T. Orton, 2019: The structure of tropical Sumatra squalls. *Weather*, **74**, 176–181, https://doi.org/10.1002/wea.3375.

Cheng, Y.-M., J. Dias, G. Kiladis, Z. Feng, and L. R. Leung, 2023: Mesoscale Convective Systems Modulated by Convectively Coupled Equatorial Waves. *Geophys. Res. Lett.*, **50**, e2023GL103335, https://doi.org/10.1029/2023GL103335.

Christopoulos, C., and T. Schneider, 2021: Assessing Biases and Climate Implications of the Diurnal Precipitation Cycle in Climate Models. *Geophys. Res. Lett.*, **48**, e2021GL093017, https://doi.org/10.1029/2021GL093017.

Crook, J., and Coauthors, 2024: Impact of the Madden–Julian oscillation and equatorial waves on tracked mesoscale convective systems over southeast Asia. *Quart. J. Roy. Meteor. Soc.*, **150**, 1724–1751, https://doi.org/10.1002/qj.4667.

Dias, J., N. Sakaeda, G. N. Kiladis, and K. Kikuchi, 2017: Influences of the MJO on the space-time organization of tropical convection. *J. Geophys. Res.*, **122**, 8012–8032, https://doi.org/10.1002/2017JD026526.

Feng, Z., and Coauthors, 2021: A Global High-Resolution Mesoscale Convective System Database Using Satellite-Derived Cloud Tops, Surface Precipitation, and Tracking. *J. Geophys. Res.*, **126**, e2020JD034202, https://doi.org/10.1029/2020JD034202.

Ha, T. V., S. Uereyen, and C. Kuenzer, 2023: Agricultural drought conditions over mainland Southeast Asia: Spatiotemporal characteristics revealed from MODIS-based vegetation time-series. *Int. J. Appl. Earth Obs. Geoinf.*, **121**, 103378, https://doi.org/10.1016/j.jag.2023.103378.

Hersbach, H., and Coauthors, 2020: The ERA5 global reanalysis. *Quart. J. Roy. Meteor. Soc.*, **146**, 1999–2049, https://doi.org/10.1002/qj.3803.

Houze, R. A., 2004: Mesoscale convective systems. *Rev. Geophys.*, **42**, RG4003, https://doi.org/10.1029/2004RG000150.

——, 2018: 100 Years of Research on Mesoscale Convective Systems. *Meteor. Monogr.*, **59**, 17.1-17.54, https://doi.org/10.1175/AMSMONOGRAPHS-D-18-0001.1.

Huffman, G. J., E. F. Stocker, D. T. Bolvin, E. J. Nelkin, and J. Tan, 2023: GPM IMERG Final Precipitation L3 Half Hourly 0.1 degree x 0.1 degree V07. Goddard Earth Sciences Data and Information Services Center (GES DISC), https://doi.org/https://doi.org/10.5067/GPM/IMERG/3B-HH/07.

Ichikawa, H., and T. Yasunari, 2006: Time–Space Characteristics of Diurnal Rainfall over Borneo and Surrounding Oceans as Observed by TRMM-PR. *J. Climate*, **19**, 1238–1260, https://doi.org/10.1175/JCLI3714.1.

——, and ——, 2008: Intraseasonal Variability in Diurnal Rainfall over New Guinea and the Surrounding Oceans during Austral Summer. *J. Climate*, **21**, 2852–2868, https://doi.org/10.1175/2007JCLI1784.1.

Janowiak, J., B. Joyce, and P. Xie, 2017: GES DISC Dataset: NCEP/CPC L3 Half Hourly 4km Global (60S - 60N) Merged IR V1 (GPM_MERGIR 1). NASA Goddard Earth Sciences Data and Information Services Center, accessed June 26, 2026, https://doi.org/https://doi.org/10.5067/P4HZB9N27EKU.

Janowiak, J. E., R. J. Joyce, and Y. Yarosh, 2001: A Real-Time Global Half-Hourly Pixel-Resolution Infrared Dataset and Its Applications. *Bull. Amer. Meteor. Soc.*, **82**, 205–218, https://doi.org/10.1175/1520-0477(2001)082%3C0205:ARTGHH%3E2.3.CO;2.

LeMone, M. A., E. J. Zipser, and S. B. Trier, 1998: The Role of Environmental Shear and Thermodynamic Conditions in Determining the Structure and Evolution of Mesoscale Convective Systems during TOGA COARE. *J. Atmos. Sci.*, **55**, 3493–3518, https://doi.org/10.1175/1520-0469(1998)055%3C3493:TROESA%3E2.0.CO;2.

Lo, J. C., and T. Orton, 2016: The general features of tropical Sumatra Squalls. *Weather*, **71**, 175–178, https://doi.org/10.1002/wea.2748.

Love, B. S., A. J. Matthews, and G. M. S. Lister, 2011: The diurnal cycle of precipitation over the Maritime Continent in a high-resolution atmospheric model. *Quart. J. Roy. Meteor. Soc.*, **137**, 934–947, https://doi.org/10.1002/qj.809.

Lu, J., T. Li, and L. Wang, 2021: Precipitation Diurnal Cycle over the Maritime Continent Modulated by the Climatological Annual Cycle. *J. Climate*, **34**, 1387–1402, https://doi.org/10.1175/JCLI-D-20-0130.1.

Mapes, B. E., 1993: Gregarious Tropical Convection. *J. Atmos. Sci.*, **50**, 2026–2037, https://doi.org/10.1175/1520-0469(1993)050%3C2026:GTC%3E2.0.CO;2.

——, and R. A. Houze, 1993: Cloud Clusters and Superclusters over the Oceanic Warm Pool. *Mon. Wea. Rev.*, **121**, 1398–1416, https://doi.org/10.1175/1520-0493(1993)121%3C1398:CCASOT%3E2.0.CO;2.

——, T. T. Warner, and M. Xu, 2003: Diurnal Patterns of Rainfall in Northwestern South America. Part III: Diurnal Gravity Waves and Nocturnal Convection Offshore. *Mon. Wea. Rev.*, **131**, 830–844, https://doi.org/10.1175/1520-0493(2003)131%3C0830:DPORIN%3E2.0.CO;2.

Moncrieff, M. W., and M. J. Miller, 1976: The dynamics and simulation of tropical cumulonimbus and squall lines. *Quart. J. Roy. Meteor. Soc.*, **102**, 373–394, https://doi.org/10.1002/qj.49710243208.

Mori, S., and Coauthors, 2004: Diurnal Land–Sea Rainfall Peak Migration over Sumatera Island, Indonesian Maritime Continent, Observed by TRMM Satellite and Intensive Rawinsonde Soundings. *Mon. Wea. Rev.*, **132**, 2021–2039, https://doi.org/10.1175/1520-0493(2004)132%3C2021:DLRPMO%3E2.0.CO;2.

Neale, R., and J. Slingo, 2003: The Maritime Continent and Its Role in the Global Climate: A GCM Study. *J. Climate*, **16**, 834–848, https://doi.org/10.1175/1520-0442(2003)016%3C0834:TMCAIR%3E2.0.CO;2.

Nguyen, H., and Coauthors, 2025: Large-scale to local factors influencing Sumatra squalls affecting Singapore. *Climate Dyn.*, **63**, 286, https://doi.org/10.1007/s00382-025-07766-w.

Pandya, R. E., and D. R. Durran, 1996: The Influence of Convectively Generated Thermal Forcing on the Mesoscale Circulation around Squall Lines. *J. Atmos. Sci.*, **53**, 2924–2951, https://doi.org/10.1175/1520-0469(1996)053%3C2924:TIOCGT%3E2.0.CO;2.

Peatman, S. C., A. J. Matthews, and D. P. Stevens, 2014: Propagation of the Madden–Julian Oscillation through the Maritime Continent and scale interaction with the diurnal cycle of precipitation. *Quart. J. Roy. Meteor. Soc.*, **140**, 814–825, https://doi.org/10.1002/qj.2161.

——, ——, and ——, 2015: Propagation of the Madden–Julian Oscillation and scale interaction with the diurnal cycle in a high-resolution GCM. *Climate Dyn.*, **45**, 2901–2918, https://doi.org/10.1007/s00382-015-2513-5.

——, C. E. Birch, J. Schwendike, J. H. Marsham, C. Dearden, S. Webster, R. R. Neely, and A. J. Matthews, 2023: The Role of Density Currents and Gravity Waves in the Offshore Propagation of Convection over Sumatra. *Mon. Wea. Rev.*, **151**, 1757–1777, https://doi.org/10.1175/MWR-D-22-0322.1.

——, ——, ——, ——, E. Howard, S. J. Woolnough, J. M. Mustafa, and A. J. Matthews, 2025: Physical Controls on the Variability of Offshore Propagation of Convection From Sumatra. *J. Geophys. Res.*, **130**, e2024JD042458, https://doi.org/10.1029/2024JD042458.

Rotunno, R., J. B. Klemp, and M. L. Weisman, 1988: A Theory for Strong, Long-Lived Squall Lines. *J. Atmos. Sci.*, **45**, 463–485, https://doi.org/10.1175/1520-0469(1988)045%3C0463:ATFSLL%3E2.0.CO;2.

Sakaeda, N., G. Kiladis, and J. Dias, 2017: The Diurnal Cycle of Tropical Cloudiness and Rainfall Associated with the Madden–Julian Oscillation. *J. Climate*, **30**, 3999–4020, https://doi.org/10.1175/JCLI-D-16-0788.1.

——, ——, and ——, 2020: The Diurnal Cycle of Rainfall and the Convectively Coupled Equatorial Waves over the Maritime Continent. *J. Climate*, **33**, 3307–3331, https://doi.org/10.1175/JCLI-D-19-0043.1.

Tang, S., P. Gleckler, S. Xie, J. Lee, M.-S. Ahn, C. Covey, and C. Zhang, 2021: Evaluating the Diurnal and Semidiurnal Cycle of Precipitation in CMIP6 Models Using Satellite- and Ground-Based Observations. *J. Climate*, **34**, 3189–3210, https://doi.org/10.1175/JCLI-D-20-0639.1.

Vincent, C. L., and T. P. Lane, 2016: Evolution of the Diurnal Precipitation Cycle with the Passage of a Madden–Julian Oscillation Event through the Maritime Continent. *Mon. Wea. Rev.*, **144**, 1983–2005, https://doi.org/10.1175/MWR-D-15-0326.1.

Watters, D., A. Battaglia, and R. P. Allan, 2021: The Diurnal Cycle of Precipitation according to Multiple Decades of Global Satellite Observations, Three CMIP6 Models, and the ECMWF Reanalysis. *J. Climate*, **34**, 5063–5080, https://doi.org/10.1175/JCLI-D-20-0966.1.

Weisman, M. L., and R. Rotunno, 2004: "A Theory for Strong Long-Lived Squall Lines" Revisited. *J. Atmos. Sci.*, **61**, 361–382, https://doi.org/10.1175/1520-0469(2004)061%3C0361:ATFSLS%3E2.0.CO;2.

Wheeler, M. C., and H. H. Hendon, 2004: An All-Season Real-Time Multivariate MJO Index: Development of an Index for Monitoring and Prediction. *Mon. Wea. Rev.*, **132**, 1917–1932, https://doi.org/10.1175/1520-0493(2004)132%3C1917:AARMMI%3E2.0.CO;2.

Wu, P., M. Hara, J. Hamada, M. D. Yamanaka, and F. Kimura, 2009: Why a Large Amount of Rain Falls over the Sea in the Vicinity of Western Sumatra Island during Nighttime. *J. Appl. Meteor. Climatol.*, **48**, 1345–1361, https://doi.org/10.1175/2009JAMC2052.1.

Yamada, H., K. Yoneyama, M. Katsumata, and R. Shirooka, 2010: Observations of a Super Cloud Cluster Accompanied by Synoptic-Scale Eastward-Propagating Precipitating Systems over the Indian Ocean. *J. Atmos. Sci.*, **67**, 1456–1473, https://doi.org/10.1175/2009JAS3151.1.

Yanase, A., K. Yasunaga, and H. Masunaga, 2017: Relationship between the direction of diurnal rainfall migration and the ambient wind over the Southern Sumatra Island. *Earth Space Sci.*, **4**, 117–127, https://doi.org/10.1002/2016EA000181.

Yang, G.-Y., and J. Slingo, 2001: The Diurnal Cycle in the Tropics. *Mon. Wea. Rev.*, **129**, 784–801, https://doi.org/10.1175/1520-0493(2001)129%3C0784:TDCITT%3E2.0.CO;2.

Yokoi, S., S. Mori, F. Syamsudin, U. Haryoko, and B. Geng, 2019: Environmental Conditions for Nighttime Offshore Migration of Precipitation Area as Revealed by In Situ Observation off Sumatra Island. *Mon. Wea. Rev.*, **147**, 3391–3407, https://doi.org/10.1175/MWR-D-18-0412.1.

You, Z., and Y. Deng, 2022: A Hierarchical Dissection of Multiscale Forcing on the Springtime Mesoscale Convective Systems in the United States. *J. Climate*, **36**, 39–54, https://doi.org/10.1175/JCLI-D-22-0150.1.

——, ——, Y. Ming, and W. Dong, 2024: A multiscale assessment of the springtime U.S. mesoscale convective systems in the NOAA GFDL AM4. *Climate Dyn.*, **62**, 4017–4030, https://doi.org/10.1007/s00382-024-07114-4.